

A COMPUTER–ASSISTED PROOF OF Σ_3 -CHAOS IN THE FORCED DAMPED PENDULUM EQUATION*

BALÁZS BÁNHÉLYI[†], TIBOR CSENDES[‡], BARNABAS M. GARAY[§], AND
LÁSZLÓ HATVANI[¶]

Abstract. The present paper is devoted to studying Hubbard’s pendulum equation

$$\ddot{x} + 10^{-1}\dot{x} + \sin(x) = \cos(t).$$

Using rigorous/interval methods of computation, the main assertion of Hubbard on chaos properties of the induced dynamics is raised from the level of experimentally observed facts to the level of a theorem completely proved. A special family of solutions is shown to be chaotic in the sense that, on consecutive time intervals $(2k\pi, 2(k+1)\pi)$ ($k \in \mathbb{Z}$), individual members of the family can freely “choose” between the following possibilities: the pendulum either crosses the bottom position exactly once clockwise or does not cross the bottom position at all or crosses the bottom position exactly once counterclockwise. The proof follows the topological index/degree approach by Mischaikow, Mrozek, and Zgliczynski. The new feature of this paper is a definition of the transition graph for which the periodic orbit lemma – the key technical result of the approach mentioned above – turns out to be a consequence of Brouwer’s fixed point theorem. The role of wholly automatic versus ‘trial-and-error with human overheads’ computer procedures in detecting chaos is also discussed.

Key words. forced damped pendulum, Σ_3 -chaos, computer-aided proof, transition graph, interval arithmetic

AMS subject classifications. 34C28, 37D45, 70K40, 70K55, 65G30

1. Introduction and the main results. The complexity of the solutions to the forced damped pendulum equation

$$m\ell\ddot{x} + b\dot{x} + mg\sin(x) = A\cos(\omega t)$$

and of related systems is one of the most frequently studied problems in dynamics. For certain values of the parameters, small perturbation theory can be applied to prove chaotic behaviour.

However, a purely theoretical approach can hardly lead to a proof for chaos if small perturbation methods break down such as in the case where

$$(1.1) \quad \ddot{x} + 10^{-1}\dot{x} + \sin(x) = \cos(t)$$

(i.e., for parameters $m\ell = mg = A = \omega = 1$ and $b = 10^{-1}$) investigated by Hubbard [24]. Based on numerical experiments and the accompanying abstract considerations mimicking Smale’s geometric horseshoe construction, Hubbard [24] made the existence

*This work was supported by the Hungarian National Science Foundation Grants OTKA No. T 048377, T 046822, T037491, and T049516. The first author is grateful for the Ferenc Deák Scholarship No. DFÖ 19/2007.

[†]Institute of Informatics, University of Szeged, H-6701 Szeged P.O. Box 652, Hungary (banely@inf.u-szeged.hu).

[‡]Institute of Informatics, University of Szeged, H-6701 Szeged P.O. Box 652, Hungary (csendes@inf.u-szeged.hu).

[§]Department of Mathematics, Budapest University of Technology, H-1521 Budapest, Hungary and Computer and Automation Institute (SZTAKI), Hungarian Academy of Sciences, H-1111 Budapest, Hungary (garay@math.bme.hu).

[¶]Bolyai Institute of Mathematics, University of Szeged, H-6701 Szeged P.O. Box 428, Hungary and Analysis and Stochastics Research Group of the Hungarian Academy of Sciences (hatvani@math.u-szeged.hu).

of Σ_3 -chaos—both on Poincaré sections of the 2π -solution mapping and also in more natural terms of the dynamics—quite plausible. His main result can be stated as follows:

THEOREM H (J.H. Hubbard [24]). *Suppose we are given a biinfinite sequence $\{\varepsilon_k\}_{k \in \mathbf{Z}} \in \{-1; 0; 1\}^{\mathbf{Z}}$, arbitrarily chosen. Then the pendulum governed by equation (1.1) has at least one motion that corresponds to the biinfinite sequence $\{\varepsilon_k\}_{k \in \mathbf{Z}}$ in the sense that, during the time interval $(2k\pi, 2(k+1)\pi)$, the pendulum bob*

- *crosses the bottom position exactly once clockwise if and only if $\varepsilon_k = -1$,*
- *does not cross the bottom position at all if and only if $\varepsilon_k = 0$,*
- *crosses the bottom position exactly once counterclockwise if and only if $\varepsilon_k = 1$,*

and does not point downwards at the time instants $t = 2k\pi$, $k \in \mathbf{Z}$.

THE FIRST AIM OF THIS PAPER is to interpret Hubbard’s observation within the Mischaikow-Mrozek framework of computer-assisted proofs for horseshoe-type chaos. We use the word ‘observation’ because, as is written on page 755 of [24], “no statement is proved anywhere”. Hubbard arranges numerical evidence according to the framework of symbolic dynamics. We complete his work by filling in the gaps via refinements of some of his theoretical arguments (in particular, by introducing the small quadrangles L_ℓ, M_ℓ, R_ℓ , $\ell \in \mathbf{Z}$) and performing the necessary rigorous interval arithmetics computations. We will show that Theorem H is a consequence of a technical result based on Figure 10 in Hubbard [24], which shows images and preimages of three large quadrangles, the convex hulls of the smaller sets $L_\ell \cup M_\ell \cup R_\ell$, $\ell = -1, 0, 1$. In short, the observation is turned into a theorem.

THEOREM 1.1. *There exist compact pairwise disjoint quadrangles*

$$L_0, M_0, R_0 \subset \{(x, \dot{x}) \in \mathbf{R}^2 \mid 0 < x < 2\pi\}$$

with the following properties. Given a biinfinite sequence $\{\varepsilon_k\}_{k \in \mathbf{Z}} \in \{-1; 0; 1\}^{\mathbf{Z}}$, there exists a solution $x = x(\{\varepsilon_k\}_{k \in \mathbf{Z}}) : \mathbf{R} \rightarrow \mathbf{R}$ to equation (1.1) such that

$$(1.2) \quad (x(2k\pi), \dot{x}(2k\pi)) \in \begin{cases} L_{\sigma_k} & \text{if } \varepsilon_k = -1 \\ M_{\sigma_k} & \text{if } \varepsilon_k = 0 \\ R_{\sigma_k} & \text{if } \varepsilon_k = 1 \end{cases}$$

where $\sigma_{k+1} = \sigma_k + \varepsilon_k$, $k \in \mathbf{Z}$ with $\sigma_0 = 0$ and

$$(1.3) \quad L_\ell = L_0 + (2\ell\pi, 0), \quad M_\ell = M_0 + (2\ell\pi, 0), \quad R_\ell = R_0 + (2\ell\pi, 0), \quad \ell \in \mathbf{Z}.$$

Quadrangles L_0, M_0 , and R_0 are shown in Figure 2.2. Property (1.2) means that the horizontal $2\ell\pi$ -translates L_ℓ, M_ℓ, R_ℓ of the carefully-chosen quadrangles L_0, M_0, R_0 are visited by trajectories of the Poincaré mapping

$$\Pi : \mathbf{R}^2 \rightarrow \mathbf{R}^2, \quad (x(0), \dot{x}(0)) \rightarrow (x(2\pi), \dot{x}(2\pi))$$

in the given order prescribed by the biinfinite sequence $\{\varepsilon_k\}_{k \in \mathbf{Z}}$. The underlying circle of abstract topological results on transition graphs and iterates of continuous mappings are the key parts of the landmark paper by Mischaikow and Mrozek [30] and of the great number of contributions that followed. The essence of the Mischaikow-Mrozek approach is to prove the existence of an abundance of combinatorially different periodic orbits and then, by using the density of periodic orbits in the shift dynamics, to pass to the existence of horseshoe-type chaos. The main technical tool is represented

by what we call Lemma 2.1 in Section 2 below. Lemma 2.1 relates to transition graphs and periodic orbits in two dimensions and constitutes the main step in proving Theorem 1.1.

THE SECOND AIM OF THIS PAPER is to provide an elementary proof of a higher-dimensional generalization of Lemma 2.1. Higher dimensional versions of Lemma 2.1 were given by Gidea and Zgliczynski [21] and Pireddu and Zanolin [37]. The underlying definitions of the transition graphs in [21] and [37] (the latter being motivated by [25]) are different. However, both proofs are based on Brouwer degree arguments. Here we will give a third definition of the transition graph in higher dimensions—the two-dimensional case having been settled by Papini and Zanolin [34]—where a simple application of Brouwer’s fixed point theorem suffices. This implies, in particular, that in some of the earliest computer-assisted proofs for horseshoe-type chaos [30], [52], [53], [54], Conley index and/or Brouwer degree arguments can be replaced by applications of Brouwer’s fixed point theorem. See also Remark 1.

The computer-aided parts of the proofs of Theorems 1.1 and H were performed in the LINUX and Cygwin environments, on a typical modern PC. We used the PROFIL/BIAS [27] programming environment which supports interval arithmetics and the Validated Numerical ODE (VNODE) package by Ned Nedialkov [32], [33]. Our basic references for rigorous/interval computation and set-valued numerics are [1] and [13], respectively.

The computer program used for the proof can be downloaded from the web page www.inf.u-szeged.hu/~banhelyi/FDP together with a short introduction and screenshots of the installation procedure.

THIS PAPER IS ORGANIZED AS FOLLOWS. Section 2 begins with a definition of the transition graph in two dimensions, goes on to state Lemma 2.1, and ends with a proof of Theorem 1.1. Theorem H and a higher dimensional generalization of Lemma 2.1 are proved in Sections 4 and 5, respectively. Connections to a 4D neural networks model are investigated in Section 6. Section 3 is devoted to a discussion of the role of the computer in chaos detection.

The results on symbolic dynamics and various forms of the pendulum equation can be found in a variety of papers. Two early results in this direction concern the standard pendulum equation with damping and variable length (but without an external forcing term) $\ddot{x} + b\dot{x} + (1 + c\sin(\mu t))\sin(x) = 0$. They were obtained by applying Melnikov’s approach [48] and a computer-assisted version of the shooting method [23], respectively. The concept of a chaotic oscillation for the case $b = 0$ was defined in [17]. For the singularly perturbed van der Pol equation $\varepsilon\ddot{x} + \varphi(x)\dot{x} + \varepsilon x = p(t)$, where φ and p are piecewise constant, the existence of embedded symbolic dynamics was proved by Mark Levi [28] in 1981. He used Newhouse’s abstract results on homoclinic bifurcations.

From the enormous (and still mathematically sound) literature on chaos in electrical circuits, we refer to the computer-assisted proofs of Galias [18] for chaos in Chua’s circuit as well as to the computer-assisted proof of Yang and Li [47] for chaos in Josephson junctions.

Chaos results for the time-periodic nonlinear Hill equation $\ddot{x} + q(t)g(x) = 0$ were obtained by topological and variational methods. The slightly more general time-periodic equations $\ddot{x} + b\dot{x} + q(t)g(x) = 0$ and $\ddot{x} + \partial W(t, x)/\partial x = h(t)$ were investigated in [7] and [6], respectively. For details, generalizations, and more references, see the forthcoming survey by Papini and Zanolin [35]. Note that Hubbard’s pendulum equation (1.1) is not included in their discussions of theoretical and computational

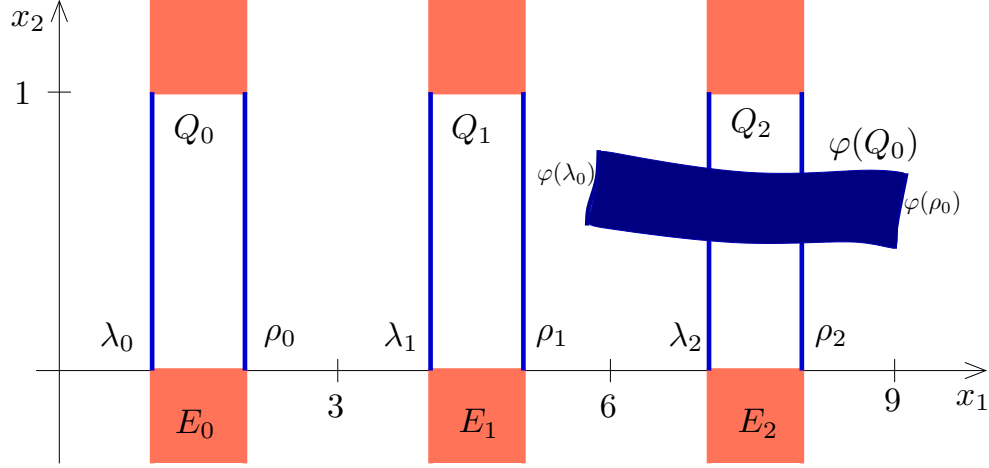


FIG. 2.1. Notation used to define the transition graph in two dimensions

results, however.

2. Transition graph and chaos associated. For $j \in \mathbb{Z}$, define

$$\begin{aligned} Q_j &= \{(x_1, x_2) \in \mathbb{R}^2 \mid 3j+1 \leq x_1 \leq 3j+2, 0 \leq x_2 \leq 1\}, \\ \lambda_j &= \{x \in Q_j \mid x_1 = 3j+1\}, \quad \rho_j = \{x \in Q_j \mid x_1 = 3j+2\}, \\ E_j &= \{(x_1, x_2) \in \mathbb{R}^2 \mid 3j+1 \leq x_1 \leq 3j+2, |2x_2 - 1| > 1\}. \end{aligned}$$

Let $X = \cup_{j \in \mathbb{Z}} Q_j \subset \mathbb{R}^2$ and consider a continuous mapping $\varphi : X \rightarrow \mathbb{R}^2$ with coordinate functions φ_1, φ_2 . The *transition graph* $\mathcal{G}(\varphi)$ of φ is defined as a directed graph with vertex set $\mathbf{V}(\mathcal{G}) = \mathbb{Z}$. For $j, \tilde{j} \in \mathbf{V}(\mathcal{G})$, the pair (j, \tilde{j}) belongs to the edge set $\mathbf{E}(\mathcal{G})$ of $\mathcal{G}(\varphi)$ if

$$(2.1) \quad \varphi(Q_j) \subset \mathbb{R}^2 \setminus \text{cl}(E_{\tilde{j}})$$

and one of the following conditions holds true:

$$(2.2) \quad \varphi_1(x) < 3\tilde{j} + 1 \text{ for } x \in \lambda_j \text{ and } \varphi_1(x) > 3\tilde{j} + 2 \text{ for } x \in \rho_j$$

or

$$(2.3) \quad \varphi_1(x) > 3\tilde{j} + 2 \text{ for } x \in \lambda_j \text{ and } \varphi_1(x) < 3\tilde{j} + 1 \text{ for } x \in \rho_j.$$

Sets $Q_j, \lambda_j, \rho_j, E_j$ ($j = 0, 1, 2$) as well as relation $(0, 2) \in \mathbf{E}(\mathcal{G})$ are shown in Figure 2.1. We write $\mathbf{V} = \mathbf{V}(\mathcal{G}) = \mathbb{Z}$ and $\mathbf{E} = \mathbf{E}(\mathcal{G})$ in the following. For $N \in \mathbb{N}$, the directed graph $\mathcal{C} = \mathcal{C}(j_0, j_1, \dots, j_N)$ is a *directed $(N+1)$ -circle in $\mathcal{G}(\varphi)$* if $\mathbf{V}(\mathcal{C}) = \{j_0, j_1, \dots, j_N\} \subset \mathbb{Z}$ and, with the convention $j_{N+1} = j_0$, $\mathbf{E}(\mathcal{C}) = \{(j_k, j_{k+1})\}_{k=0}^N \subset \mathbf{E}$. The directed graph $\mathcal{P} = \mathcal{P}(\{j_k \mid k \in \mathbb{Z}\})$ is a *directed biinfinite path in $\mathcal{G}(\varphi)$* if $\mathbf{V}(\mathcal{P}) = \{j_k \mid k \in \mathbb{Z}\} \subset \mathbb{Z}$ and $\mathbf{E}(\mathcal{P}) = \{(j_k, j_{k+1})\}_{k \in \mathbb{Z}} \subset \mathbf{E}$. The definition of directed finite and infinite paths (i.e. paths having a root vertex) in $\mathcal{G}(\varphi)$ follows a similar pattern and will not be included here.

LEMMA 2.1. *Let $\mathcal{C} = \mathcal{C}(j_0, j_1, \dots, j_N)$ be a directed circle in the transition graph $\mathcal{G}(\varphi)$. Then there is a finite sequence of points $\{q_k\}_{k=0}^N \subset X$ such that, with the*

convention $q_{N+1} = q_0$,

$$q_{k+1} = \varphi(q_k) \quad \text{and} \quad q_k \in Q_{j_k} \quad , \quad k = 0, 1, \dots, N .$$

Actually, Lemma 2.1 comes from the paper by Mischaikow and Mrozek [30]. As stated above, it is a version of the main result in Zgliczynski [52]. The formulation and the proof of a higher-dimensional generalization of Lemma 2.1 will be postponed until Section 5.

COROLLARY 2.2. *Let $\mathcal{P} = \mathcal{P}(\{j_k\}_{k \in \mathbb{Z}})$ be a directed biinfinite path in the transition graph $\mathcal{G}(\varphi)$. Assume that either*

(A) *every directed infinite path in \mathcal{P} has infinitely many different vertices*

or

(B) *\mathcal{G} (as a directed graph) is connected.*

Then there is a biinfinite sequence of points $\{q_k\}_{k \in \mathbb{Z}} \subset X$ with the property that

$$q_{k+1} = \varphi(q_k) \quad \text{and} \quad q_k \in Q_{j_k} \quad , \quad k \in \mathbb{Z} .$$

Proof. Case (A). Choose a positive integer $\ell = L$ and consider the finite path with consecutive vertices $(j_{-L}, j_{-L+1}, \dots, j_L) \in \mathbb{Z}^{2L+1}$. Next, choose an integer $M > L$ such that $j_M \neq j_k$ for $k = -L, \dots, L$. Redefining φ on Q_{j_M} , we may assume that $(j_M, j_{-L}) \in \mathbf{E}$. Thus the extended finite sequence $(j_{-L}, \dots, j_L, j_{L+1}, \dots, j_M) \in \mathbf{V}^{L+1+M}$ forms the set of consecutive vertices of a directed circle in $\mathcal{G}(\varphi)$. Applying Lemma 2.1, we conclude there must exist a finite sequence of points $\{q_k^L\}_{|k| \leq L} \subset X$ such that

$$q_{k+1}^L = \varphi(q_k^L) \quad \text{for} \quad k = -L, \dots, L-1 \quad \text{and} \quad q_k^L \in Q_{j_k} \quad \text{for} \quad k = -L, \dots, L .$$

Repeating the previous considerations for $\ell = L+1, L+2, \dots$, a standard Bolzano-Weierstrass subsequence argument in the limiting process $\ell \rightarrow \infty$ leads to the desired result.

Case (B). The connectedness of \mathcal{G} is equivalent to the property that every directed finite path in \mathcal{P} is contained in a directed circle of $\mathcal{G}(\varphi)$. Consequently, with some minor modifications, the argument we applied in proving case (A) can be repeated here. \square

Corollary 2.2 asserts the existence of a φ -trajectory which visits the Q_j 's in the prescribed order: a directed biinfinite path of type (A) or (B) of the transition graph is shadowed by a φ -trajectory. Directed $(N+1)$ -circles in $\mathcal{G}(\varphi)$ are shadowed by $(N+1)$ -periodic φ -trajectories. This is the essence of Lemma 2.1.

Remark 1. If $N = 0$, then Lemma 2.1 simplifies to the Colorado fixed point theorem in [3]. If the vertical coordinate is missing, then Lemma 2.1 simplifies to a well-known result in one-dimensional dynamics (see, for example Lemma III.1.4 in [40]) whose proof is based solely on the intermediate value theorem. The proof of a higher dimensional generalization of Lemma 2.1 in Section 5 mimics the standard derivation of the Miranda theorem from Brouwer's fixed point theorem [36]. Note that the Miranda theorem is nothing else but the higher dimensional counterpart of the intermediate value theorem. It is known to be equivalent to Brouwer's fixed point theorem and to many other important results in topology [51]. Its history can be traced back to Poincaré and Bohl. Not long ago, the Miranda theorem appeared as a root test in numerical analysis and interval computation [16], [15], [42] as well as in

chaos theory for two-dimensional mappings [34], [4]. The ‘rectangular nature’ of the Miranda theorem fits in beautifully with the rectangles used to define the transition graph as well as the rectangles used in rigorous/interval computation.

Remark 2. Observe that Lemma 2.1 remains valid if the right hand side of inclusion (2.1) is weakened to $\mathbb{R}^2 \setminus E_j$ and the strict inequalities in (2.2) and (2.3) are replaced by their nonstrict counterparts. (In fact, for $\ell = 1, 2, \dots$, it is elementary to construct a modified map $\varphi^\ell : X \rightarrow \mathbb{R}^2$ satisfying $|\varphi^\ell - \varphi| < 1/\ell$ for which Lemma 2.1 (as stated above) applies. Allowing $\ell \rightarrow \infty$, the existence of the desired φ -periodic trajectory follows from the Bolzano-Weierstrass argument.) The reason for stating Lemma 2.1 in the form presented above is to make the result stable with respect to small perturbations. Actually, if the conditions of Lemma 2.1 are met, and a continuous mapping $\tilde{\varphi} : \cup_{j \in \mathbb{Z}} Q_j \rightarrow \mathbb{R}^2$ satisfies $\max\{|\varphi(q) - \tilde{\varphi}(q)| \mid q \in \cup_{k=0}^N Q_{j_k}\} \leq \eta$ with η sufficiently small, then the $(N+1)$ -tuple $(j_0, j_1, \dots, j_N) \in \mathbb{Z}^{N+1}$ forms a directed circle in $\mathcal{G}(\tilde{\varphi})$ as well. As we shall see below, it is exactly this robustness property of the transition graph which makes Lemma 2.1 so suitable in computer-assisted proofs for horseshoe-type chaos. Stability in small perturbations in turn ensures stability in numerical approximations, including those with rounding errors.

Now we shall return to equation (1.1) studied by Hubbard [24].

In what follows we will demonstrate how Corollary 2.2 applies and how it leads to a complete proof of Theorem 1.1. The strategy is to find a biinfinite sequence of pairwise disjoint compact sets $\{K_j\}_{j \in \mathbb{Z}}$ in the Poincaré plane $\{(x, \dot{x}) \in \mathbb{R}^2\}$ such that, up to a coordinate transformation h , Corollary 2.2 applies to the associated Poincaré mapping $\Pi : (x(0), \dot{x}(0)) \rightarrow (x(2\pi), \dot{x}(2\pi))$ of equation (1.1). We need a homeomorphism h of the Poincaré plane onto the standard plane $\{(x_1, x_2) \in \mathbb{R}^2\}$ such that, for

$$\varphi = h\Pi h^{-1}|X : X \rightarrow \mathbb{R}^2 \quad \text{with} \quad Q_j = h(K_j), \quad j \in \mathbb{Z},$$

Corollary 2.2 directly applies. Here, of course, $X = \cup_{j \in \mathbb{Z}} Q_j$ and $h\Pi h^{-1}|X$ means the restriction of $h\Pi h^{-1}$ to X . Since Π is 2π -periodic in the x variable and the number of different ε_k 's is three, the biinfinite sequence $\{K_j\}_{j \in \mathbb{Z}}$ is sought as a collection of the horizontal $2\ell\pi$ -translates of the three specially-chosen quadrangles L_0, M_0, R_0 (compare the notation in (1.3) and see Figure 2.2) with

$$K_{3\ell} = L_0 + (2\ell\pi, 0), \quad K_{3\ell+1} = M_0 + (2\ell\pi, 0), \quad K_{3\ell+2} = R_0 + (2\ell\pi, 0), \quad \ell \in \mathbb{Z}.$$

Given a biinfinite sequence $\{\varepsilon_k\}_{k \in \mathbb{Z}} \in \{-1; 0; 1\}^{\mathbb{Z}}$, it is essential that the directed biinfinite path $\mathcal{P} = \mathcal{P}(\{j_k\}_{k \in \mathbb{Z}})$ with $j_k = 3\sigma_k + 1 + \varepsilon_k$ (where—as defined in Theorem 1.1— $\sigma_0 = 0$ and $\sigma_{k+1} = \sigma_k + \varepsilon_k$ for $k \in \mathbb{Z}$) be a subgraph of $\mathcal{G}(\varphi)$. Applying Corollary 2.2, trajectories satisfying (1.2) correspond to the directed biinfinite path $\mathcal{P} = \mathcal{P}(\{j_k\}_{k \in \mathbb{Z}})$ and vice versa.

Proof. [Proof of Theorem 1.1.] The successful realization of the strategy outlined above depends on the careful choice of the quadrangles L_0, M_0, R_0 and of the coordinate transformation h . Noting the horizontal 2π -translation invariance property of the collection $\{K_j\}_{j \in \mathbb{Z}}$, the continuous mapping $\varphi = h\Pi h^{-1}|X$ is prescribed to be 9-periodic with respect to the x_1 variable. This can be guaranteed by requiring that the coordinate functions of homeomorphism $h : \{(x, \dot{x}) \in \mathbb{R}^2\} \rightarrow \{(x_1, x_2) \in \mathbb{R}^2\}$ satisfy

$$(2.4) \quad h_1(x + 2\pi, \dot{x}) = 9 + h_1(x, \dot{x}) \quad \text{and} \quad h_2(x + 2\pi, \dot{x}) = h_2(x, \dot{x}).$$

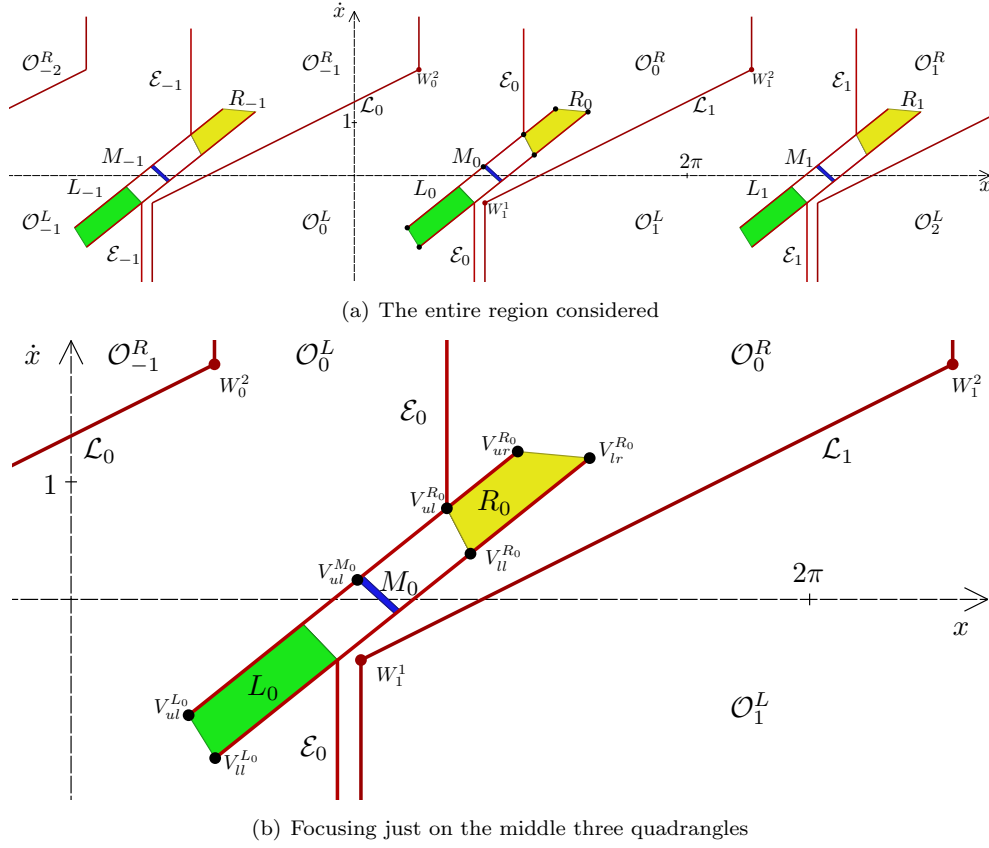


FIG. 2.2. Notation used in proving Theorem 1.1

The existence of quadrangles L_0, M_0, R_0 that lead to a *transition graph suitably complex* depends on the inner structure of the Poincaré mapping.

Following Hubbard [24], define quadrangles $K_0 = L_0, K_1 = M_0, K_2 = R_0$ as

$$K_j = \text{conv}\{V_{ul}^{K_j}, V_{ur}^{K_j}, V_{ll}^{K_j}, V_{lr}^{K_j}\}, \quad j = 0, 1, 2,$$

which are the closed convex hulls of their respective upper left, upper right, lower left, lower right vertices. (The letters L, M , and R stand for left, middle, and right, respectively.) The coordinates of these vertices are

$$\begin{aligned} V_{ul}^{L_0} &= (1.000, -0.985) & V_{ur}^{L_0} &= (1.970, -0.208) \\ V_{ll}^{L_0} &= (1.226, -1.350) & V_{lr}^{L_0} &= (2.226, -0.516), \end{aligned}$$

$$\begin{aligned} V_{ul}^{M_0} &= (2.436, 0.166) & V_{ur}^{M_0} &= (2.481, 0.201) \\ V_{ll}^{M_0} &= (2.758, -0.123) & V_{lr}^{M_0} &= (2.796, -0.092), \end{aligned}$$

$$\begin{aligned} V_{ul}^{R_0} &= (3.197, 0.775) & V_{ur}^{R_0} &= (3.800, 1.258) \\ V_{ll}^{R_0} &= (3.398, 0.389) & V_{lr}^{R_0} &= (4.412, 1.202). \end{aligned}$$

See Figure 2.2. For details on how the individual vertices were found, see the third paragraph of Section 3 below.

Now consider the broken line in Figure 2.2, namely

$$\mathcal{L}_1 = \{\text{the vertical half-line below } W_1^1\} \cup [W_1^1, W_1^2] \cup \{\text{the vertical half-line above } W_1^2\}$$

where

$$W_1^1 = (w_1^1, w_2^1) = V_{lr}^{L_0} + (0.2, 0) \quad , \quad W_1^2 = (w_1^2, w_2^2) = (7.5, 2)$$

and $[W_1^1, W_1^2]$ stands for the closed line segment between W_1^1 and W_1^2 . The open strip between \mathcal{L}_1 and the translated broken line $\mathcal{L}_0 = \mathcal{L}_1 + (-2\pi, 0)$ shall be denoted by \mathcal{S}_0 . Now with ‘conv’ standing for the closed convex hull of the points in braces, define

$$\begin{aligned} \mathcal{D}_0 = & \{\text{the vertical half-line below } V_{lr}^{L_0}\} \cup L_0 \cup \text{conv}\{V_{ur}^{L_0}, V_{ul}^{M_0}, V_{lr}^{M_0}, V_{lr}^{L_0}\} \\ & \cup M_0 \cup \text{conv}\{V_{ur}^{M_0}, V_{ul}^{R_0}, V_{lr}^{R_0}, V_{lr}^{M_0}\} \cup R_0 \cup \{\text{the vertical half-line above } V_{ul}^{R_0}\}. \end{aligned}$$

The open strips between \mathcal{D}_0 and \mathcal{L}_0 (resp. \mathcal{L}_1) will be denoted by \mathcal{O}_0^L (resp. \mathcal{O}_0^R). The union of the right-hand side boundary of the strip \mathcal{O}_0^L and the left-hand side boundary of the strip \mathcal{O}_0^R will be denoted by \mathcal{B}_0 . Finally, we let

$$\mathcal{E}_0 = \mathcal{B}_0 \setminus \{(V_{ul}^{L_0}, V_{lr}^{L_0}) \cup (V_{ur}^{R_0}, V_{lr}^{R_0})\},$$

where, for example, $(V_{ul}^{L_0}, V_{lr}^{L_0})$ stands for the open line segment connecting $V_{ul}^{L_0}$ and $V_{lr}^{L_0}$. (The closed line segment connecting $V_{ul}^{L_0}$ and $V_{lr}^{L_0}$, for example, will be denoted by $[V_{ul}^{L_0}, V_{lr}^{L_0}]$. Note that \mathcal{E}_0 is the union of ten closed line segments and two closed half-lines. See Figure 2.2 again.)

The crucial properties responsible for the edge structure of the transition graph are

$$(2.5) \quad \Pi(R_{-1}), \Pi(M_0), \Pi(L_1) \subset \mathcal{S}_0 \setminus \mathcal{E}_0,$$

$$(2.6) \quad \Pi([V_{ul}^{R_{-1}}, V_{ul}^{R_{-1}}]), \Pi([V_{ul}^{M_0}, V_{ul}^{M_0}]), \Pi([V_{ur}^{L_1}, V_{lr}^{L_1}]) \subset \mathcal{O}_0^L,$$

$$(2.7) \quad \Pi([V_{ur}^{R_{-1}}, V_{lr}^{R_{-1}}]), \Pi([V_{ur}^{M_0}, V_{lr}^{M_0}]), \Pi([V_{ul}^{L_1}, V_{ul}^{L_1}]) \subset \mathcal{O}_0^R.$$

See Figure 2.3 showing the sets $\Pi(L_0)$ (a translated copy of $\Pi(L_1)$), $\Pi(M_0)$, $\Pi(R_0)$ (a translated copy of $\Pi(R_{-1})$). The subset relations (2.5), (2.6), (2.7) will be checked by computer. Note that the sets $\mathcal{S}_0 \setminus \mathcal{E}_0$, \mathcal{O}_0^L , \mathcal{O}_0^R are open and all the nine sets $\Pi(R_{-1})$, \dots , $\Pi([V_{ul}^{L_1}, V_{ul}^{L_1}])$ on the respective left-hand sides are compact. Hence inclusions (2.5), (2.6), (2.7) remain valid if the entire construction is repeated with the sets \mathcal{D}_0 , \mathcal{B}_0 , and \mathcal{E}_0 slightly thicker; that is, if \mathcal{D}_0 , \mathcal{B}_0 , and \mathcal{E}_0 are replaced by their closed neighborhoods \mathcal{D} , \mathcal{B} , and \mathcal{E} , suitably chosen.

Next we will start constructing a homeomorphism h subject to condition (2.4). We also require that $Q_j = h(K_j)$ with

$$\begin{aligned} (3j+1, 1) &= h(V_{ul}^{K_j}), \quad (3j+2, 1) = h(V_{ur}^{K_j}), \quad j = 0, 1, 2 \\ (3j+1, 0) &= h(V_{ul}^{K_j}), \quad (3j+2, 0) = h(V_{lr}^{K_j}), \quad j = 0, 1, 2 \end{aligned}$$

(i.e., the corresponding vertices are mapped to each other) and

$$(2.8) \quad \text{cl}(E_0 \cup E_1 \cup E_2) \subset h(\mathcal{E}) \quad , \quad \{(x_1, x_2) \in \mathbb{R}^2 \mid x_1 = 0\} = h(\mathcal{L}_0).$$

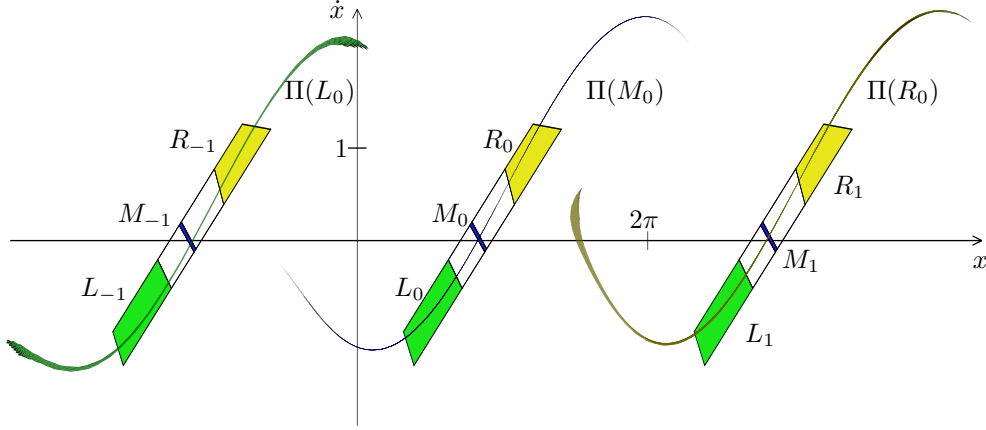


FIG. 2.3. Images of the specially-chosen quadrangles under Π

Due to the piecewise linear boundaries of the sets involved, the construction of h is elementary. We have a fair amount of freedom in choosing h . Advanced results of two-dimensional topology are not needed for this. Note that, by translation symmetry, the broken line \mathcal{L}_1 is mapped onto the line of equation $x_1 = 9$.

Recall that $X = \cup_{j \in \mathbb{Z}} Q_j$. Then property (2.5) and the inclusion in (2.8) imply that

$$\varphi(X) \subset \mathbb{R}^2 \setminus \text{cl}(\cup_{j \in \mathbb{Z}} E_j) .$$

Using (2.6), (2.7), we conclude that the transition graph of φ is as follows. The vertex set of $\mathcal{G}(\varphi)$ is obviously $\mathbf{V} = \mathbb{Z}$ and $\mathcal{G}(\varphi)$ is three-periodic in the sense that $(j, \tilde{j}) \in \mathbf{E}$ if and only if $(j + 3, \tilde{j} + 3) \in \mathbf{E}$. The edges starting from the vertex subset $\{0, 1, 2\}$ are like those shown in Figure 2.4(a):

$$(0, -3); (0, -2); (0, -1); (1, 0); (1, 1); (1, 2); (2, 3); (2, 4); (2, 5) .$$

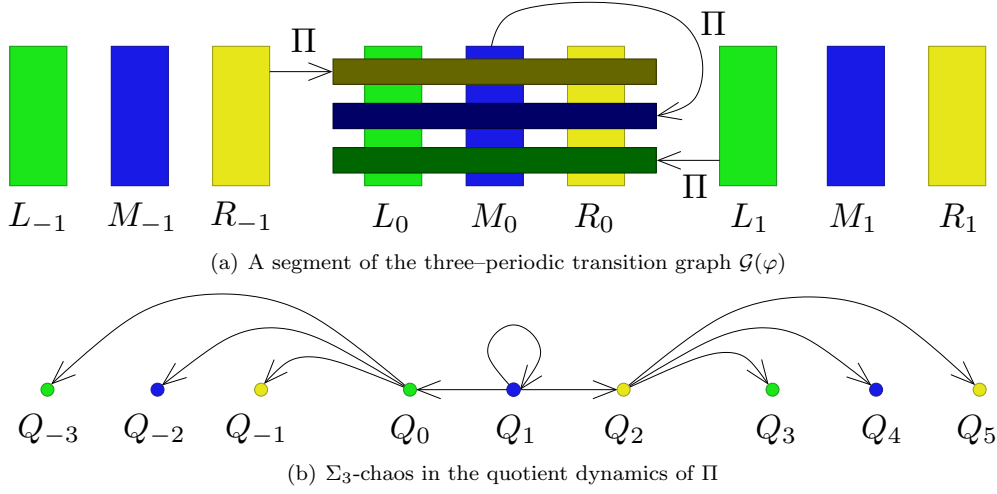
Thus we arrive at the schematic phase portrait of the Poincaré mapping depicted in Figure 2.4(b).

Given a biinfinite sequence $\{\varepsilon_k\}_{k \in \mathbb{Z}} \in \{-1; 0; 1\}^{\mathbb{Z}}$, a quick analysis of the transition graph $\mathcal{G}(\varphi) = \mathcal{G}(h\Pi h^{-1}|X)$ shows that the directed biinfinite path $\mathcal{P} = \mathcal{P}(\{j_k\}_{k \in \mathbb{Z}})$ with $j_k = 3\sigma_k + 1 + \varepsilon_k$ (where—as defined in Theorem 1.1— $\sigma_0 = 0$ and $\sigma_{k+1} = \sigma_k + \varepsilon_k$ for $k \in \mathbb{Z}$) is a subgraph of $\mathcal{G}(\varphi)$. Trajectories satisfying (1.2) correspond to the directed biinfinite path $\mathcal{P} = \mathcal{P}(\{j_k \mid k \in \mathbb{Z}\})$ and vice versa.

This provides all the necessary points for proving Theorem 1.1: apply Corollary 2.2 then we are done. \square

The derivation of Theorem 1.1 follows the main argument in the Mischaikow-Mrozek framework for computer-assisted proofs. (Note that the invertibility of Π was not exploited, but it will be needed for the backward invariance of the set Λ in Corollary 2.3 below). For the geometric background and details on the role of the computer, see Section 3.

It is not hard to reformulate Theorem 1.1 in the language of symbolic dynamics [49], [40]. In fact, recall that $Q_j = h(K_j)$ and let $\Theta \subset X$ be the closure of all periodic points of φ that shadow the directed circles of $\mathcal{G}(\varphi)$. The set Θ is backward and

FIG. 2.4. *Combinatorial complexity in Hubbard's forced damped pendulum equation*

forward invariant under φ . For $x \in \Theta$, the formula

$$(c(x))_k = j_k, \quad \text{whenever } \varphi^k(x) \in Q_{j_k} \text{ and } k \in \mathbb{Z},$$

defines a continuous itinerary mapping $c : \Theta \rightarrow \mathbb{Z}^{\mathbb{Z}}$. The inverse of a homeomorphism h lifts everything to the Poincaré plane. Clearly $\Lambda = h^{-1}(\Theta)$ is backward and forward invariant under the Poincaré mapping Π and, for $\lambda = (x, \dot{x}) \in \Lambda$ with $d(\lambda) = c(h(\lambda))$,

$$(d(\lambda))_k = j_k \quad \text{whenever } \Pi^k(\lambda) \in K_{j_k}, \quad k \in \mathbb{Z}.$$

Letting S denote the shift operator on $\mathbb{Z}^{\mathbb{Z}}$, we may conclude that

$$c(\varphi(x)) = Sc(x) \quad \text{for each } x \in \Theta \quad \text{and} \quad d(\Pi(\lambda)) = Sd(\lambda) \quad \text{for each } \lambda \in \Lambda.$$

The entire construction is based on the horizontal 2π -translation symmetry of Π . The respective quotient maps are continuous and satisfy

$$\bar{d}(\bar{\Pi}(\bar{\lambda})) = \bar{S}\bar{d}(\bar{\lambda}) \quad \text{for each } \bar{\lambda} \in \bar{\Lambda}.$$

The quotient transition graph $\mathcal{G}(\bar{\varphi})$ is the complete directed graph on three vertices and thus the modulo 3 itinerary map $\bar{d} : \bar{\Lambda} \rightarrow \{0, 1, 2\}^{\mathbb{Z}}$ is onto. In particular, note that

$$(\bar{d}(\bar{\lambda}))_k = 1 + \varepsilon_k \quad \text{for } \bar{\lambda} \in \bar{\Lambda} = \Lambda \cap \{(x, \dot{x}) \in \mathbf{R}^2 \mid 0 < x < 2\pi\}, \quad k \in \mathbb{Z}.$$

The quotient results can be expressed in compact form as a corollary.

COROLLARY 2.3 (A continuation of Theorem 1.1). *The modulo 2π Poincaré mapping $\bar{\Pi}$ on $\bar{\Lambda}$ is semiconjugate to the shift operator \bar{S} on Σ_3 , the space of three symbols.*

In fact, as suggested by Hubbard [24], \bar{d} is plausibly one-to-one and thus $\bar{\Pi}|_{\bar{\Lambda}}$ and \bar{S} are conjugate. See Figure 2.3 again and compare it with Figure 2.4(a) and Figure 2.4(b).

3. Chaos detection by computer. What the computer is used for in the Mischaikow–Mrozek framework of computer-assisted proofs for chaos is *to check certain subset relations* (like (2.5), (2.6), (2.7)) and above all, *to find the subset relations to be checked* — in essence, to find a collection of ‘rectangular’ subsets of the phase space like L_0, M_0, R_0 such that the associated transition graph has at least two different, but intersecting circles. The hard part is to find the subset relations to be checked. If small perturbation arguments do not help, one cannot get by without a computer. The checking part is much easier and sometimes, in exceptional cases, like the equation $\ddot{x} + x = \sin(\sqrt{2}t) + 2^{-1}(|5x + 1| - |5x - 1|)$ [38], it can be done by hand. Still, the proof in [38] is computer-assisted. The successful collection of ‘rectangular’ subsets is the result of trial-and-error computer experimentation with human overheads.

It is natural to ask to what extent the task of finding the successful subset relations can be left to the computer. The required subset relations determine a constrained satisfaction problem [10] and techniques of global optimization [39] apply. If we want to look for three quadrangles, the search domain of the optimization procedure is a subset of a 24-dimensional parameter space (8 dimensions for each quadrangle based on the coordinate pairs of the four vertices; the search for a successful collection of the ‘forbidden sets’ $\mathcal{L}_0, \mathcal{L}_1$, and \mathcal{E}_0 requires the introduction of some additional parameters). And the smaller the search domain, the better. However, a ‘small’ search domain corresponds to a ‘good’ initial guess which can only be obtained from some *a priori* known theoretical or numerical results on the details of the dynamics. Typical candidates for members of a successful collection are quadrangles situated on the unstable manifold of a transversal homoclinic saddle.

In an interesting paper devoted to Hénon mapping with the classical parameters $a = 1.4$ and $b = 0.3$, Galias [19] describes the configuration of 29 polygons which leads to the rigorous entropy estimate $h(\mathcal{H}) > 0.430\dots$, which is quite close to the generally accepted value of $h(\mathcal{H}) = 0.465\dots$. All the 29 polygons are narrow quadrangles—or quadrangles with some vertices ‘chopped off’—situated along the unstable manifold of the homoclinic saddle. They were found by hand, based on an earlier search for periodic points of low periods. The well-known and highly automatized GIAO package [12], [13] is used to construct 247 GIAO polygons in a forthcoming paper by Day, Frongillo and Trevino [11] proving the slightly better estimate of $h(\mathcal{H}) > 0.4318\dots$ (If a global search is performed just on finding 29 or 247 segments of the unstable manifold, one needs 58 or 494 parameters, respectively. The second number is far too much for optimization methods currently available for this type of problem.) Nevertheless, it remains open whether a bootstrap application of global optimization procedures, keeping the number of parameters under 10 say, at each step of the gradual improvements along the consecutive local searches, can achieve a better estimate. We feel it is not inappropriate here to call to the attention of the reader a forthcoming paper [5] of ours where, within a 17-dimensional parameter space, the full power of the optimization method [4] is exploited. The main result is that \mathcal{H}^k , the k -th iterate of Hénon’s mapping with the classical parameters $a = 1.4$ and $b = 0.3$ has an embedded copy of the Σ_2 dynamics if and only if $k = 2, k = 4$, or $k \geq 6$. This is guaranteed by Smale’s abstract theory of transversal homoclinic saddles only for $k \geq k_0$, sufficiently large. (Incidentally, all existence proofs (like [31], [14], [20]) for a transversal homoclinic saddle in the dynamics of \mathcal{H} are, to the best of our knowledge, in some way or other, computer-assisted.)

In proving Theorem 1.1, the vertices of quadrangles L_0, M_0, R_0 (as well as of the

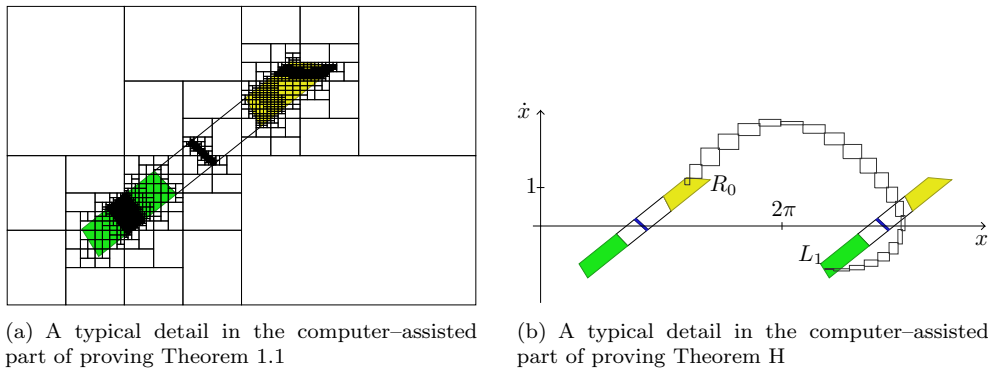
‘forbidden sets’ $\mathcal{L}_0, \mathcal{L}_1, \mathcal{E}_0$) were chosen in the way shown in Hubbard [24]. Though the coordinates of the individual vertices were not explicitly given by him, it was straightforward to adjust them based on Figure 10 of his paper. This adjustment was made by hand. According to our estimates, our method [10] would have required several months of CPU time. Actually, what Hubbard works with are just three large quadrangles, the convex hulls of which we define as the sets $L_\ell \cup M_\ell \cup R_\ell$, $\ell = -1, 0, 1$, and the ‘forbidden sets’ are not mentioned by him at all. At first sight, it is quite plausible that the twelve vertices $V_{ul}^{L_0}, \dots, V_{lr}^{R_0}$ lie on the circumference of Hubbard’s large quadrangle. However, we could not find such an arrangement. This indicates the differences between nonrigorous and rigorous computation. Just like the Hénon mapping \mathcal{H} , the Poincaré mapping Π of Hubbard’s pendulum equation (1.1) also has a homoclinic saddle. This saddle point is

$$P = (2.634\dots, 0.026\dots) \quad \text{with eigenvalues} \quad \mu_1 = 321.836\dots \quad \text{and} \quad \mu_2 = 0.001\dots$$

(all our computations being rigorous). Of course P represents an unstable 2π -periodic solution which has bifurcated from the upward/top equilibrium position $x = \pi, \dot{x} = 0$ of the damped unforced pendulum. Equation (1.1) has a second, asymptotically stable 2π -periodic solution which corresponds to the sink $Q = (4.236\dots, 0.392\dots)$ of the Poincaré mapping with eigenvalues $\mu_{1,2} = -0.725\dots \pm i 0.129\dots$ and which has bifurcated from the bottom equilibrium position $x = 0, \dot{x} = 0$ of the damped unforced pendulum. Computer-assisted reasoning shows there are no further 2π -periodic solutions. Note that P is contained in M_0 and, its unstable manifold intersects the carefully-chosen quadrangles in the rather strange order of $R_{-1}, M_{-1}, L_{-1}, L_0, M_0, R_0, L_1, M_1, R_1$.

Unstable and stable manifolds of P intersect each other outside P . Apparently, this is a transversal intersection. But we did not verify transversality by rigorous computation. The reason is that transversality by itself, though guaranteeing the existence of a topological horseshoe, contains less information about the dynamics than a transition graph with carefully chosen ‘rectangular’ subsets. The next logical step forward should be, rather, the verification of the Conley-Moser invariant cone field conditions [49] leading (if it is really the case) to transversality as well as to the conjugacy between $\bar{\Pi}|\bar{\Lambda}$ and \bar{S} . Unfortunately, *the verification of inclusions (2.5), (2.6), (2.7) takes almost an hour on a typical modern PC*. See Figure 4.1(a). Because of this, we think there is little hope of checking the invariant cone field conditions in a reasonable amount of time. Nevertheless, the semiconjugacy of $\bar{\Pi}|\bar{\Lambda}$ to \bar{S} established in Corollary 2.3 is not much worse than the conjugacy we expected. Semiconjugacy to \bar{S} means that the dynamics is at least as complex as the full shift on the space of three symbols, while conjugacy would mean that the dynamics of $\bar{\Pi}|\bar{\Lambda}$ is just as complex as the one belonging to \bar{S} . What can be shown is that $m(\bar{\Lambda})$, the Lebesgue measure of $\bar{\Lambda}$, is zero. (This is clear because $\bar{\Pi}(\bar{C}) \subset \bar{C}$ for $\bar{C} = \{(x, \dot{x}) \in \mathbb{R}^2 \mid 0 \leq x < 2\pi, |\dot{x}| \leq 12\}$, $\bar{\Lambda} \subset \bigcap_{k=0}^{\infty} \bar{\Pi}^k(\bar{C})$, and $\bar{\Pi}$ contracts areas by a factor of $e^{-\pi/5}$, due to damping and the Liouville theorem [24].) Questions on additional chaos properties in Hubbard’s pendulum equation (1.1)—like the Wada property experimentally observed by Hubbard [24] or fine ergodic properties like the existence of a unique SRB measure (found for the Lorenz equation by Tucker [46]) and mixing (found for the Lorenz equation by Luzzato, Melbourne, and Paccaut [29])—remain open.

In conclusion, we note that the existence of a transition graph with two different but intersecting circles is implicit in a paper by Stoffer and Palmer [44] on shadowing. In essence, they prove that the existence of two hyperbolic periodic orbits which come

FIG. 4.1. *Checking inclusions by interval computation*

sufficiently near each other without remaining too close for a long time (e.g. those whose minimal periods are highly nonresonant) implies the existence of an embedded horseshoe. This corresponds to the Levinson phenomenon which motivated Smale to construct the geometric horseshoe [43], [28]. For a comparison between the shadowing and the topological approach in computer-assisted proofs for chaos, see the recent paper by Coomes, Kocak, and Palmer [9].

4. Chaos in natural terms of the dynamics. The one-to-one correspondence between a set of the solutions to Hubbard's pendulum equation (1.1) and the set of all biinfinite sequences on three symbols manifests itself in natural terms of the dynamics.

Focusing on the pendulum, the quadrangles L_0 , M_0 , R_0 remain hidden, even to the most observant viewer. What can be easily seen, are high speeds or low speeds, the number of consecutive clockwise or counterclockwise returns, changes in the direction of swing and/or rotation, and movements across the upper and/or the lower vertical position. When systematizing a range of dynamical behaviour, the mind has a tendency to consider the consecutive occurrences of alternative, easily discernible events like a heads-or-tails sequence in coin-tossing.

Theorems H and 1.1 should be interpreted from this point of view. Any possible order of the mutually exclusive alternatives can occur. Both observations describe the same combinatorial aspect of Σ_3 -chaos, the existence of 'coin-tossing' (coins with three sides) label sequences [26] for itineraries. However, the alternatives in Theorem 1.1 are hard to observe whereas the alternatives in Theorem H are quite transparent. There exist uncountably many solutions of Hubbard's pendulum equation which can be distinguished from each other based on their combinatorially different qualitative behaviour. This is what we might call combinatorial chaos in natural terms of the dynamics. Previous examples include symbolic dynamics in terms of consecutive return times in Alekseev's three-body system [2], [24]; consecutive maxima and minima in the Lorenz systems [22]; the number of sign changes in consecutive time intervals of equal length [7], [45]; and multibumps in bursting oscillations [41]. Their natural place is in the vicinity of bifurcating homoclinic/heteroclinic orbit connections.

Proof. [Proof of Theorem H.] In order to prove Theorem H we need to examine what the solution map $(x(0), \dot{x}(0)) \rightarrow (x(t), \dot{x}(t))$ does between the Poincaré sections at $t_0 = 0$ and $t_1 = 2\pi$.

First, consider the collection of motions of the forced damped pendulum with initial position $(x(0), \dot{x}(0)) \in R_0$ and final position $(x(2\pi), \dot{x}(2\pi)) \in L_1 \cup M_1 \cup R_1$. It

is not hard to check by rigorous/interval computation that $0 < x(t) < 4\pi$, whenever $0 \leq t \leq 2\pi$, and

$$\{(x(t), \dot{x}(t)) \in \mathbb{R}^2 \mid 0 \leq t \leq 2\pi\} \cap \{(x, \dot{x}) \in \mathbb{R}^2 \mid x = 2\pi \text{ and } \dot{x} \leq 0\} = \emptyset.$$

Applying the intermediate value theorem, it follows that $x(t^*) = 2\pi$ for some $t^* \in (0, 2\pi)$, $x(t) \in (0, 2\pi)$ for $t \in [0, t^*)$, and $x(t) \in (2\pi, 4\pi)$ for $t \in (t^*, 2\pi]$. In other words, during the time interval $(0, 2\pi)$, the pendulum bob crosses the bottom position exactly once counterclockwise and does not point downwards at the time instants $t_0 = 0$ and $t_1 = 2\pi$. This holds true for motions of the pendulum with initial position $(x(0), \dot{x}(0)) \in R_0$ and final position $(x(2\pi), \dot{x}(2\pi)) \in L_1 \cup M_1 \cup R_1$ (but not for all motions with initial position $(x(0), \dot{x}(0)) \in R_0$). This holds true especially for all $\sigma_0 = 0$, $\varepsilon_0 = 1$ (and, a fortiori, $\sigma_1 = 1$, $\varepsilon_1 \in \{-1, 0, 1\}$) motions of the pendulum described by Theorem 1.1. Parts of the necessary computations in subcase $\sigma_0 = 0$, $\varepsilon_0 = 1$, $\sigma_1 = 1$, $\varepsilon_1 = -1$ are shown in Figure 4.1(b).

The remaining cases $\sigma_0 = 0$, $\varepsilon_0 = 0$ and $\sigma_0 = 0$, $\varepsilon_0 = -1$ were settled in a similar way. *The total CPU time requested was under two minutes on a typical modern PC.* \square

The connection between symbolic dynamics and oscillation patterns in equation (1.1) is worth further investigation. We would like to know whether symbolic dynamics appears regarding the crossing the bottom *and the top* equilibrium position.

5. Lemma 2.1 in a higher dimension. A simple proof. Let m, n be fixed nonnegative integers, and let $\mathbf{V} \subset \mathbb{Z}$ be a finite or countably infinite indexing set. Next, let the boundary and interior of a compact set S in a Euclidean space \mathbb{R}^k be denoted by ∂S and $\text{int}(S)$, respectively. The closed neighborhood of radius $R > 0$ of a point p and a set S in \mathbb{R}^k will be denoted by $\mathcal{B}^k[p, R]$ and $\mathcal{B}^k[S, R]$, respectively. The norm and scalar product in \mathbb{R}^k shall be denoted by $\|\cdot\|$ and $\langle \cdot, \cdot \rangle$.

Now consider the collection of rectangular sets of the form

$$Q_j = \{x = (u, s) \in \mathbb{R}^m \times \mathbb{R}^n \mid u \in U_j, s \in S_j\}, \quad j \in \mathbf{V},$$

where $\{U_j\}_{j \in \mathbf{V}}$ and $\{S_j\}_{j \in \mathbf{V}}$ are compact topological balls in \mathbb{R}^m and in \mathbb{R}^n , respectively. Note that S_j is a retract of \mathbb{R}^n . Let $r_j : \mathbb{R}^n \rightarrow S_j$ be a retraction, where $j \in \mathbf{V}$.

Next, let $X = \cup_{j \in \mathbf{V}} Q_j \subset \mathbb{R}^m \times \mathbb{R}^n$ and consider a continuous mapping $\varphi : X \rightarrow \mathbb{R}^m \times \mathbb{R}^n$ with coordinate functions φ_u, φ_s . After, suppose that $Q_j \cap Q_k = \emptyset$ for $j \neq k$ and that $\{j \in \mathbf{V} \mid Q_j \cap \{(u, s) \in \mathbb{R}^m \times \mathbb{R}^n \mid \|u\| + \|s\| < R\} \neq \emptyset\}$ is finite for any $R > 0$.

The *transition graph* $\mathcal{G}(\varphi)$ of φ is defined as a directed graph with vertex set \mathbf{V} . For $\tilde{j}, \hat{j} \in \mathbf{V}$, the pair (\tilde{j}, \hat{j}) belongs to the edge set \mathbf{E} of $\mathcal{G}(\varphi)$ if

$$(5.1) \quad \varphi(Q_{\tilde{j}}) \subset \mathbb{R}^m \times \mathbb{R}^n \setminus U_{\hat{j}} \times (\mathbb{R}^n \setminus S_{\hat{j}})$$

and, for some positive constants $\eta_0 = \eta_0(\tilde{j}, \hat{j})$ and $\kappa_0 = \kappa_0(\tilde{j}, \hat{j})$, one of the following two conditions holds true:

$$(5.2) \quad \begin{aligned} &v_j + \kappa(u_{\tilde{j}} - \varphi_u(v_j, s_j)) \in U_{\hat{j}} \quad \text{whenever} \\ &v_j \in U_{\tilde{j}}, d(v_j, \partial U_{\tilde{j}}) \leq \eta_0, s_j \in S_{\tilde{j}}, u_{\tilde{j}} \in U_{\tilde{j}} \quad \text{and} \quad 0 \leq \kappa \leq \kappa_0 \end{aligned}$$

or

$$(5.3) \quad \begin{aligned} &v_j - \kappa(u_{\tilde{j}} - \varphi_u(v_j, s_j)) \in U_{\hat{j}} \quad \text{whenever} \\ &v_j \in U_{\tilde{j}}, d(v_j, \partial U_{\tilde{j}}) \leq \eta_0, s_j \in S_{\tilde{j}}, u_{\tilde{j}} \in U_{\tilde{j}} \quad \text{and} \quad 0 \leq \kappa \leq \kappa_0. \end{aligned}$$

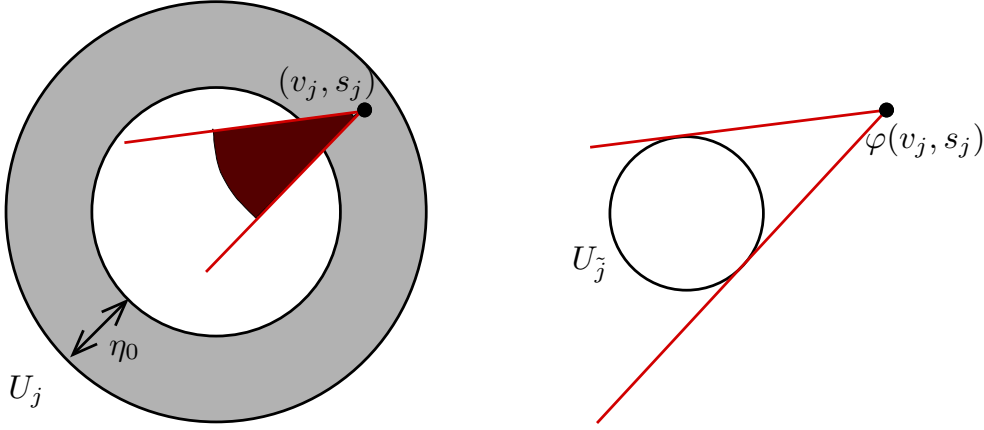


FIG. 5.1. Condition (5.2) for fixed $(v_j, s_j) \in \{u_j \in U_j \mid d(u_j, \partial U_j) \leq \eta_0\} \times S_j$

The definition of the transition graph in Section 2 is more restrictive. If $m = n = 1$, then condition (5.1) is equivalent to $\varphi(Q_j) \subset \mathbb{R}^2 \setminus E_{\tilde{j}}$, a weakening of condition (2.1) discussed in Remark 2. Similarly, with $\eta_0 = 1 - \vartheta_0$ and κ_0 suitably chosen (it is enough to make both $\vartheta_0 > 0$ and $\kappa_0 = \kappa_0(\vartheta_0) > 0$ sufficiently small), conditions (5.2) and (5.3) are implied by conditions (2.2) and (2.3), respectively.

With the notion of the transition graph redefined in $\mathbb{R}^m \times \mathbb{R}^n$, $m, n \geq 1$, the wording of Lemma 2.1 in higher dimension coincides with that of the original Lemma 2.1 verbatim. Now we turn to the proof of this generalization. Conditions (5.2) and (5.3) will be clarified and analyzed later on.

Proof. [Proof of Lemma 2.1 in $\mathbb{R}^m \times \mathbb{R}^n$.] The strategy is to rewrite the system of equations

$$x_{k+1} = \varphi(x_k) \quad \text{and} \quad x_k \in Q_{j_k} \quad , \quad k = 0, 1, \dots, N$$

as a fixed point equation $(x_0, x_1, \dots, x_N) = \mathcal{F}(x_0, x_1, \dots, x_N)$ in the product space $\prod_{k=0}^N Q_{j_k} \subset (\mathbb{R}^m \times \mathbb{R}^n)^{N+1}$ and to check that all conditions of Brouwer's fixed point theorem are satisfied.

Choose a positive constant

$$\kappa^* \leq \min_{k=0,1,\dots,N} \kappa_0(j_k, j_{k+1}) \quad \text{such that} \quad \kappa^* C^* \leq \min_{k=0,1,\dots,N} \eta_0(j_k, j_{k+1}),$$

where

$$C^* = \max_{k=0,1,\dots,N} \max\{\|u_{k+1} - \varphi_u(x_k)\| \mid u_{k+1} \in U_{j_{k+1}}, x_k \in Q_{j_k}\}.$$

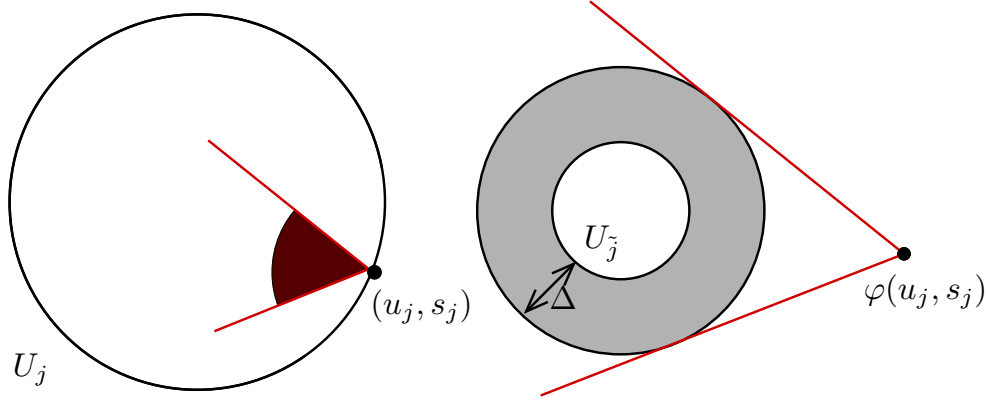
For $(x_0, x_1, \dots, x_N) \in \prod_{k=0}^N Q_{j_k}$, coordinatewise we set

$$(\mathcal{F}(x_0, x_1, \dots, x_N))_k = (u_k + \varepsilon_k \kappa^* (u_{k+1} - \varphi_u(x_k)), r_{j_k}(\varphi_s(x_{k-1}))) \in \mathbb{R}^m \times \mathbb{R}^n.$$

Here ε_k depends on the pair $(j, \tilde{j}) = (j_k, j_{k+1})$ taking $\varepsilon_k = 1$ if condition (5.2) applies and $\varepsilon_k = -1$ if condition (5.3) applies, where $k = 0, 1, \dots, N$.

Since $x_{N+1} = x_0$, $x_{-1} = x_N$ by convention, we shift the index values in the \mathbb{R}^n -coordinate, and see that the fixed point equation $(x_0, x_1, \dots, x_N) = \mathcal{F}(x_0, x_1, \dots, x_N)$ in $\prod_{k=0}^N Q_{j_k}$ is equivalent to the system of equations

$$(5.4) \quad u_{k+1} = \varphi_u(x_k) \quad \text{and} \quad s_{k+1} = r_{j_{k+1}}(\varphi_s(x_k)) \quad , \quad k = 0, 1, \dots, N.$$

FIG. 5.2. Condition (5.6) for fixed $(u_j, s_j) \in \partial U_j \times S_j$

In view of condition (5.1), the first identity in (5.4) implies that $\varphi_s(x_k) \in S_{j_{k+1}}$. Hence $r_{j_{k+1}}(\varphi_s(x_k)) = \varphi_s(x_k)$, and system (5.4) simplifies to

$$u_{k+1} = \varphi_u(x_k) \quad \text{and} \quad s_{k+1} = \varphi_s(x_k), \quad \text{i.e.,} \quad x_{k+1} = \varphi(x_k), \quad k = 0, 1, \dots, N.$$

It is clear that $\prod_{k=0}^N Q_{j_k}$ is a compact topological ball in $(\mathbb{R}^m \times \mathbb{R}^n)^{N+1}$ and $\mathcal{F} : \prod_{k=0}^N Q_{j_k} \rightarrow (\mathbb{R}^m \times \mathbb{R}^n)^{N+1}$ is a continuous function. Here all that remains is for us to prove that

$$(\mathcal{F}(x_0, x_1, \dots, x_N))_k \in Q_{j_k} \quad \text{whenever} \quad (x_0, x_1, \dots, x_N) \in \prod_{k=0}^N Q_{j_k},$$

$k = 0, 1, \dots, N$. Since $r_{j_k}(\varphi_s(x_{k-1})) \in S_{j_k}$, we can go to the \mathbb{R}^m -coordinate and just check that

$$(5.5) \quad u_k + \varepsilon_k \kappa^* (u_{k+1} - \varphi_u(x_k)) \in U_{j_k} \quad \text{if} \quad x_k = (u_k, s_k) \in Q_{j_k} \quad \text{and} \quad u_{k+1} \in U_{j_{k+1}}.$$

If $u_k \in U_{j_k}$ with $d(u_k, \partial U_{j_k}) \leq \eta_0(j_k, j_{k+1})$, then—depending on the value of ε_k —(5.5) reduces to (5.2) or (5.3) with $\kappa = \kappa^*$. On the other hand, if $u_k \in U_{j_k}$ with $d(u_k, \partial U_{j_k}) > \eta_0(j_k, j_{k+1})$, then (5.5) follows from the inequality $\kappa^* \|u_{k+1} - \varphi_u(x_k)\| \leq \kappa^* C^* \leq \eta_0(j_k, j_{k+1})$, $k = 0, 1, \dots, N$. \square

From a geometric point of view, both condition (5.2) and the alternative condition (5.3) imply that U_{j_k} is ‘surrounded by’ $\varphi_u(\partial U_{j_k} \times S_{j_k})$. In the special case $U_j = U_{j_k} = \mathcal{B}^m[0, 1]$ and $S_j = \mathcal{B}^n[0, 1]$ (compact unit balls in the respective Euclidean spaces), so condition (5.2) is a consequence of the inequality

$$\langle \varphi_u(u, s) - \tilde{u}, u \rangle > 0 \quad \text{whenever} \quad u, \tilde{u} \in \mathbb{R}^m, \quad s \in \mathbb{R}^n, \quad \|u\| = 1, \quad \|\tilde{u}\|, \|s\| \leq 1$$

which resembles certain geometric conditions in various versions of Brouwer’s fixed point theorem [51].

The remaining part of this section will be devoted to a technical analysis of conditions (5.2) and (5.3). By a symmetry argument, this analysis reduces to investigating (5.2). Condition (5.2) will be replaced by the slightly stronger condition (5.6), which is stable with respect to small perturbations of φ_u , including numerical approximations with rounding errors. A second advantage of (5.6) over (5.2) is that condition

(5.6) can be readily checked. To see this, compare Figure 5.2 with Figure 5.1. Overall, condition (5.6) is better suited to computer-assisted proofs than (5.2). The section ends with the somewhat more convenient and transparent condition (5.8), where uniformity with respect to λ is not required.

PROPOSITION 5.1. *Condition (5.2) is a consequence of a simpler requirement. It is that there exist positive constants $\lambda_0 = \lambda_0(j, \tilde{j})$ and $\Delta = \Delta(j, \tilde{j})$ such that*

$$(5.6) \quad \begin{aligned} & u_j + \lambda(w_{\tilde{j}} - \varphi_u(u_j, s_j)) \in U_j \quad \text{whenever} \\ & u_j \in \partial U_j, \quad s_j \in S_j, \quad w_{\tilde{j}} \in \mathcal{B}^m[U_{\tilde{j}}, \Delta] \quad \text{and} \quad 0 \leq \lambda \leq \lambda_0. \end{aligned}$$

Proof. We omit indices j, \tilde{j} in the following and write $U = U_j$, $S = S_j$, and $W = U_{\tilde{j}}$.

Now suppose that condition (5.6) is satisfied, but (5.2) is not. Then there are sequences $\{v_\ell\} \subset U$, $\{s_\ell\} \subset S$, $\{w_\ell\} \subset W$, $\{\kappa_\ell\} \subset \mathbb{R}^+$ which have the following properties:

$$(5.7) \quad p_\ell = v_\ell + \kappa_\ell(w_\ell - \varphi_u(v_\ell, s_\ell)) \notin U, \quad \text{for } \ell = 1, 2, \dots$$

and both $v_\ell \rightarrow \partial U$ and $\kappa_\ell \rightarrow 0$ as $\ell \rightarrow \infty$.

Since $v_\ell \in U$ and $p_\ell \notin U$, there exists a $\kappa_\ell^* \in [0, \kappa_\ell]$ such that

$$z_\ell = v_\ell + \kappa_\ell^*(w_\ell - \varphi_u(v_\ell, s_\ell)) \in \partial U, \quad \text{for } \ell = 1, 2, \dots$$

With the construction, $0 < \kappa_\ell - \kappa_\ell^* \leq \lambda_0$ and (by using the uniform continuity of mapping φ_u on the compact set $U \times S$) $\|\varphi_u(z_\ell, s_\ell) - \varphi_u(v_\ell, s_\ell)\| \leq \Delta$ for ℓ large enough. In view of condition (5.6), we conclude that

$$p_\ell = z_\ell + (\kappa_\ell - \kappa_\ell^*)(w_\ell + \varphi_u(z_\ell, s_\ell) - \varphi_u(v_\ell, s_\ell)) - \varphi_u(z_\ell, s_\ell) \in U$$

for large enough ℓ , which contradicts (5.7). \square

PROPOSITION 5.2. *Actually, condition (5.6) is a consequence of a simpler requirement. It is that there exists a positive constant $\delta = \delta(j, \tilde{j})$ such that*

$$(5.8) \quad \begin{aligned} & u_j + \mu(w_{\tilde{j}} - \varphi_u(u_j, s_j)) \in \text{int}(U_j) \quad \text{whenever} \\ & u_j \in \partial U_j, \quad s_j \in S_j, \quad w_{\tilde{j}} \in \mathcal{B}^m[U_{\tilde{j}}, \delta] \quad \text{and} \quad 0 < \mu \leq \mu_0 \quad \text{with some } \mu_0 = \mu_0(u_j, s_j, w_{\tilde{j}}). \end{aligned}$$

Proof. As before, we write $U = U_j$, $S = S_j$, and $W = U_{\tilde{j}}$.

Fix $u^* \in \partial U$, $s^* \in S$ and $w^* \in W$. By compactness, it is sufficient to demonstrate the existence of two positive constants $\tau = \tau(u^*, s^*, w^*)$ and $\lambda^* = \lambda^*(u^*, s^*, w^*)$ such that, given $u \in \partial U$, $s \in S$ and $w \in \mathcal{B}^m[W, \delta]$ with $\|u - u^*\| \leq \tau$, $\|s - s^*\| \leq \tau$, $\|w - w^*\| \leq \tau$, the following holds true:

$$u + \lambda(w - \varphi_u(u, s)) \in U \quad \text{whenever } 0 \leq \lambda \leq \lambda^*.$$

By continuity, there is a $\sigma \in (0, \delta)$ such that, for arbitrary $w \in \mathcal{B}^m[w^*, \sigma]$ and $q \in U \cap \mathcal{B}^m[u^*, \sigma]$,

$$(5.9) \quad \tilde{w} - \varphi_u(q, s^*) = w - \varphi_u(u^*, s^*) \quad \text{for some } \tilde{w} \in \mathcal{B}^m[w^*, \delta].$$

In view of condition (5.8) with $(u^*, s^*, w^*) = (u_j, s_j, w_{\tilde{j}})$, we may assume that

$$u^* + \alpha_+^*(w^* - \varphi_u(u^*, s^*)) \in \text{int}(U) \cap \partial \mathcal{B}^m[u^*, \sigma] \quad \text{for some } \alpha_+^* > 0.$$

As a corollary, a simple geometric argument implies the existence of a constant $\eta \in (0, \sigma)$ such that, for arbitrary $p \in \mathcal{B}^m[u^*, \eta]$ and $w \in \mathcal{B}^m[w^*, \eta]$,

$$p + \alpha_+(w - \varphi_u(u^*, s^*)) \in \text{int}(U) \cap \partial\mathcal{B}^m[u^*, \sigma] \quad \text{for some } \alpha_+ = \alpha_+(p, w) > 0,$$

where α_+ is unique, the function $(p, w) \rightarrow \alpha_+(p, w)$ is continuous, and $\alpha_+(u^*, w^*) = \alpha_+$. For future use, we note that

$$\alpha_* = \inf\{\alpha_+(p, w) \mid p \in \mathcal{B}^m[u^*, \eta], w \in \mathcal{B}^m[w^*, \eta]\} > 0$$

by compactness. Now consider the straight line segment

$$L_{p,w} = \{p + \lambda(w - \varphi_u(u^*, s^*)) \mid \lambda \geq 0\} \cap \mathcal{B}^m[u^*, \sigma]$$

and assume that $q = p + \gamma_0(w - \varphi_u(u^*, s^*)) \in \partial U \cap L_{p,w}$ for some $\gamma_0 < \alpha_+$. Applying property (5.9), condition (5.8) (with $(q, s^*, \tilde{w}) = (u_j, s_j, w_j)$) implies that

$$p + \gamma(w - \varphi_u(u^*, s^*)) = q + (\gamma - \gamma_0)(\tilde{w} - \varphi_u(q, s^*)) \in \text{int}(U)$$

for $\gamma > \gamma_0$, where $|\gamma - \gamma_0|$ is small. By an elementary connectedness argument in one dimension, we infer that $L_{p,w} \cap U$ is a compact interval with an endpoint on $\partial\mathcal{B}^m[u^*, \sigma]$. See Figure 5.3.

Similarly, observe that there exists a constant $\tau \in (0, \eta)$ such that, for arbitrary $w \in \mathcal{B}^m[w^*, \tau]$, $u \in U \cap \mathcal{B}^m[u^*, \tau]$ and $s \in S \cap \mathcal{B}^n[s^*, \tau]$,

$$(5.10) \quad \hat{w} - \varphi_u(u^*, s^*) = w - \varphi_u(u, s) \quad \text{for some } \hat{w} \in \mathcal{B}^m[w^*, \eta].$$

If, in particular, $u \in \partial U \cap \mathcal{B}^m[u^*, \tau]$, $s \in S \cap \mathcal{B}^n[s^*, \tau]$ and $w \in \mathcal{B}^m[w^*, \tau]$, then by property (5.10)

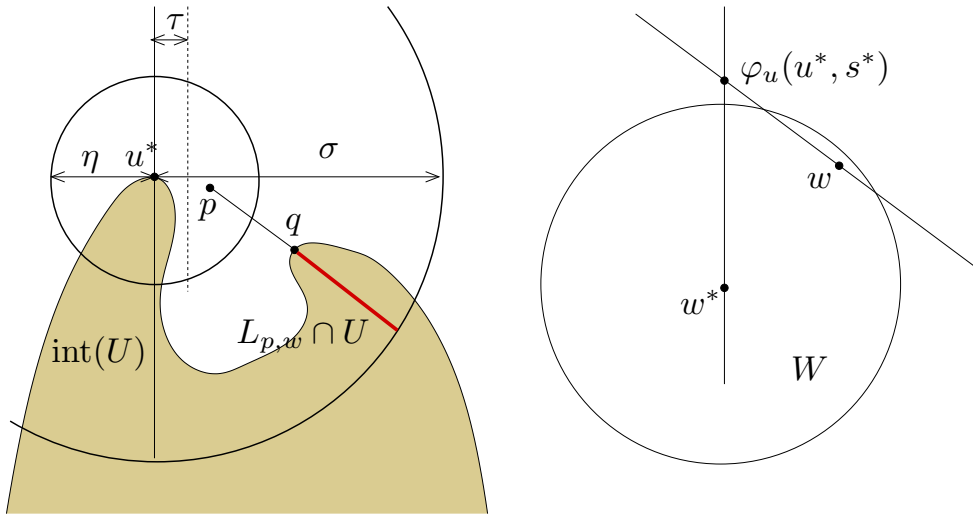
$$\{u + \lambda(w - \varphi_u(u, s)) \mid \lambda \geq 0\} \cap \mathcal{B}^m[u^*, \sigma] = L_{u, \hat{w}}$$

for some $\hat{w} \in \mathcal{B}^m[w^*, \eta]$. Since $u \in \partial U \subset U$ and $L_{u, \hat{w}} \cap U$ is a compact interval with an endpoint on $\partial\mathcal{B}^m[u^*, \sigma]$, we conclude that $L_{u, \hat{w}} \subset U$. Hence $u + \lambda(w - \varphi_u(u, s)) \in U$ for $0 \leq \lambda \leq \alpha_+(u, \hat{w})$, and thus $\lambda^* = \lambda^*(u^*, s^*, w^*)$ can be chosen for $\alpha_* > 0$. \square

We do not know whether $\text{int}(U_j)$ in (5.8) can actually be replaced by U_j . On the other hand, simple examples confirm that Proposition 5.1 does not hold true for $\Delta = 0$.

6. Lemma 2.1 and a recent 4D example of Yang and Li [50]. As we mentioned earlier, conditions (5.2) and (5.3) can be readily checked for $m = 1$, but they are more complicated for $m > 1$. Regardless of the value of the positive integer n , condition (5.1) remains rather simple. It follows that for small, multidimensional perturbations of one-dimensional mappings which ‘contract’ in the new directions, the $m = 1$, $n \geq 1$ case of Lemma 2.1 can be applied without difficulty. For example, Lemma 2.1 can be applied for the family of mappings investigated in [54] and simplifies the proofs therein.

As for the $m > 1$ case, it is reasonable to suppose that a twofold application of Lemma 2.1 leads to a rigorous proof of the existence of chaotic behaviour in a recent four-dimensional neural network example of Xiao-Song Yang and Qingdu Li [50]. Our conjecture is supported by analyzing the figures in that paper.


FIG. 5.3. *Illustration of the proof of Proposition 5.2*

We will now consider the autonomous system of ordinary differential equations [50]

$$\begin{aligned}
 \dot{x}_1 &= -x_1 + 2.10f(x_1) + 2.50f(x_2) \\
 \dot{x}_2 &= -x_2 - 2.60f(x_1) + 1.00f(x_2) + 3.00f(x_3) \\
 \dot{x}_3 &= -x_3 - 2.80f(x_2) + 0.50f(x_3) - 1.10f(x_4) \\
 \dot{x}_4 &= -100x_4 + 100f(x_3) + 160f(x_4)
 \end{aligned}
 \tag{6.1}$$

which models a cellular neural network of Chua–Roska type [8] with $f(x_i) = 2^{-1}(|x_i + 1| - |x_i - 1|)$, $x_i \in \mathbb{R}$, $i = 1, 2, 3, 4$. A horseshoe in an appropriate Poincaré mapping Π was found by Yang and Li [50] numerically, via non-rigorous computation. Their paper does not say how the 14 coefficients/weights on the right-hand side of the above system of ordinary differential equations were chosen. The nice Figure 4 in [50] suggests that the successful Poincaré section was chosen by a trial and error process with human overheads.

Now we would like to show that, with the underlying sets properly chosen, the transition graph $\mathcal{G}(\Pi)$ is the complete directed graph on two vertices. The argument will be based on case $m = 2$, $n = 1$ of the higher-dimensional generalization of Lemma 2.1 and, of course, on the geometric information contained in [50].

Simplified and schematic variants of Figures 7, 5, and 8 of [50] are presented here as Figures 6.1, 6.2, and 6.3, respectively. The two vertical prisms with quadrilateral base in [50] correspond to our cylinders $\mathcal{C}_U = U \times S$ and $\mathcal{C}_W = W \times S$, while the vertical edges of the prisms correspond to the points A_ℓ and B_ℓ , $\ell = 1, 2, 3, 4$, respectively. The prisms are strongly contracted in the vertical direction. As for the two horizontal directions within, mapping Π is a modest expansion. Applied to our situation, the crucial observation in [50] is that vertical segments on the jacket of \mathcal{C}_U and of \mathcal{C}_W (i.e., segments of the form $\{A\} \times S$ and $\{B\} \times S$ with $A \in \partial U$ and $B \in \partial W$) are mapped onto ‘almost vertical’ curves on $\partial\Pi(\mathcal{C}_U)$, and on $\partial\Pi(\mathcal{C}_W)$, respectively. This explains why $\Pi(\mathcal{C}_U)$ and $\Pi(\mathcal{C}_W)$ can be regarded as cylinders and implies that condition (5.6)

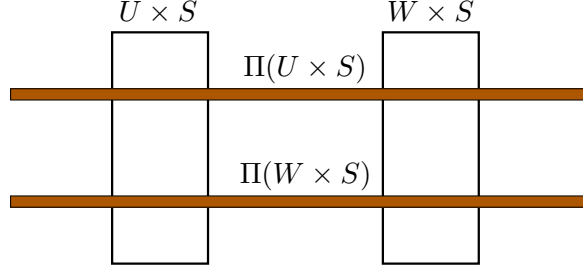


FIG. 6.1. The front view of the four cylinders $C_U = U \times S$, $C_W = W \times S$, $\Pi(C_U)$, and $\Pi(C_W)$

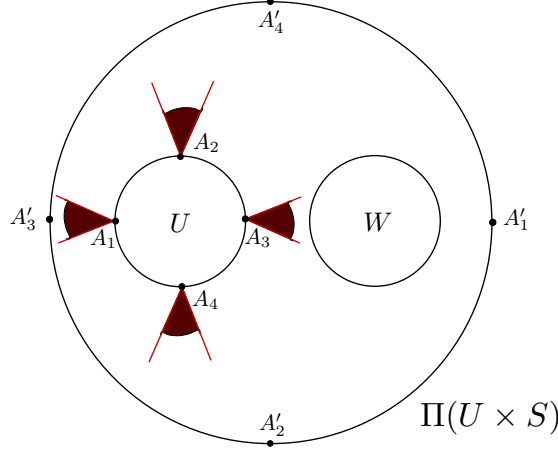


FIG. 6.2. The upper view of the cylinders $C_U = U \times S$, $\Pi(C_U)$, and $C_W = W \times S$

or its alternative counterpart (i.e., there exist positive constants λ_0 and Δ such that

$$(6.2) \quad \begin{aligned} u_j - \lambda(w_j - \varphi_u(u_j, s_j)) \in U_j & \quad \text{whenever} \\ u_j \in \partial U_j, s_j \in S_j, w_j \in \mathcal{B}^m[U_j, \Delta] & \quad \text{and } 0 \leq \lambda \leq \lambda_0 \end{aligned}$$

has to be checked only for a single $s = s^* \in S$. There is no loss of generality in assuming that $S = [-1, 1] \subset \mathbb{R}$ and $s^* = 0$. For brevity, we write $A'_\ell = \Pi_u(A_\ell, 0)$ and $B'_\ell = \Pi_u(B_\ell, 0)$, $\ell = 1, 2, 3, 4$. The relative position of the four cylinders and the 2×8 special points in Figures 6.1, 6.2, and 6.3 are exactly like the computer pictures in [50].

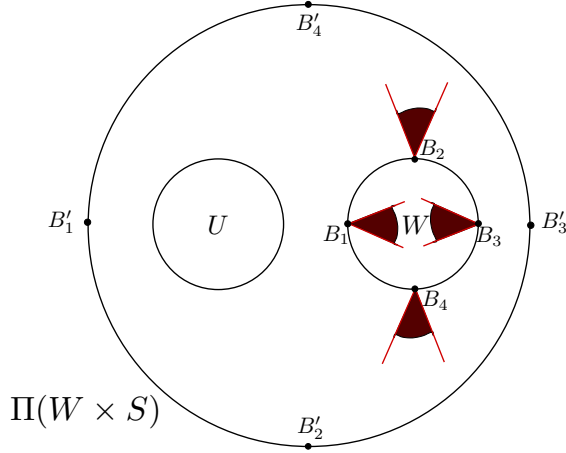
In what follows we will show that Lemma 2.1 applies in this situation. We do this by examining if and how, with $U_j = U, W$ and $U_j^- = U, W$, the alternative pair of conditions (5.6) and (6.2) is satisfied. The final result will be that, with vertex set $\mathbf{V}(\mathcal{G}) = \{C_U, C_W\}$, the edge set of the transition graph $\mathcal{G}(\Pi)$ is $\mathbf{E}(\mathcal{G}) = \{(C_U, C_U), (C_U, C_W), (C_W, C_U), (C_W, C_W)\}$.

For a fixed $\ell \in \{1, 2, 3, 4\}$, the angular sector at A_ℓ in Figure 6.2 describes the two cones

$$\{A_\ell + \lambda(u - A'_\ell) \in \mathbb{R}^2 \mid u \in \mathcal{B}^2[U, \Delta] \text{ and } 0 \leq \lambda \leq \lambda_0\}$$

and

$$\{A_\ell + \lambda(w - A'_\ell) \in \mathbb{R}^2 \mid w \in \mathcal{B}^2[W, \Delta] \text{ and } 0 \leq \lambda \leq \lambda_0\}.$$

FIG. 6.3. The upper view of the cylinders $C_W = W \times S$, $\Pi(C_W)$, and $C_U = U \times S$

(For the sake of simplicity, these two cones have been drawn in Figure 6.2 as a single angular sector with vertex A_ℓ for every ℓ . And like all of figures in this section, the small positive constants Δ and λ_0 remain unspecified.) Based on the direction of these angular sectors, it seems plausible that condition (6.2) is satisfied for $\varphi = \Pi$, $S_j = [-1, 1]$, $U_j = U$ and $U_{j+1} = U, W$. As regards the proof of Lemma 2.1, Proposition 5.1 implies that condition (5.5) is satisfied for $\varphi = \Pi$, $S_{j_k} = [-1, 1]$, $U_{j_k} = U$, $\varepsilon_k = -1$ and $U_{j_{k+1}} = U, W$.

Similarly, for $\ell = 1, 2, 3, 4$, the angular sector at B_ℓ in Figure 6.3 describes the two cones (or the union of the two cones)

$$\{B_\ell + \lambda(u - B'_\ell) \in \mathbb{R}^2 \mid u \in \mathcal{B}^2[U, \Delta] \text{ and } 0 \leq \lambda \leq \lambda_0\}$$

and

$$\{B_\ell + \lambda(w - B'_\ell) \in \mathbb{R}^2 \mid w \in \mathcal{B}^2[W, \Delta] \text{ and } 0 \leq \lambda \leq \lambda_0\}.$$

Unfortunately, neither condition (5.6) nor (6.2) is satisfied and, if left unchanged, the proof of Lemma 2.1 breaks down in the present situation. However, the direction of the four angular sectors in Figure 6.3 suggests a simple way-out.

Together with a combinatorial modification, the proof of Lemma 2.1 still holds true. The $\mathbb{R}^m = \mathbb{R}^2$ coordinate

$$u_k + \varepsilon_k \kappa^*(u_{k+1} - \varphi_u(x_k)) = u_k + \varepsilon_k \kappa^*(u_{k+1} - \Pi_u(x_k)) \in \mathbb{R}^2$$

of $(\mathcal{F}(x_0, x_1, \dots, x_N))_k$, $k = 0, 1, \dots, N$ is to be replaced by

$$(u_k^1 + \varepsilon_k^1 \kappa^*(u_{k+1}^1 - \Pi_u^1(x_k)), u_k^2 + \varepsilon_k^2 \kappa^*(u_{k+1}^2 - \Pi_u^2(x_k))) \in \mathbb{R} \times \mathbb{R},$$

where superscripts 1 (resp. 2) stand for the first(=horizontal) (resp. second(=vertical)) coordinate in Figures 6.2 and 6.3, and

$$\varepsilon_k^1 = \varepsilon_k^2 = -1 \quad \text{if } U_{j_k} = U \text{ and } U_{j_{k+1}} = U, W$$

and

$$\varepsilon_k^1 = 1, \varepsilon_k^2 = -1 \quad \text{if } U_{j_k} = W \text{ and } U_{j_{k+1}} = U, W.$$

No other changes are needed for the proof. After this refinement of the choice of parameter ε_k condition (5.5) will be satisfied again.

We feel justified to conclude that, eventually, the argument outlined above leads to a rigorous proof for the existence of embedded Σ_2 dynamics in equation (6.1). At present, several details are missing. It is not enough to check the alternative conditions for two times four points in a simplified and schematic situation. The relation between the original dynamics creating Figures 7, 5, and 8 of [50] and its simplified representation in Figures 6.1, 6.2, and 6.3 has to be analyzed rigorously. This task is parallel to the one we performed in Section 2 for Hubbard's forced damped pendulum equation (1.1).

Acknowledgements. The authors are grateful for the suggestions and comments by the referees that helped improve the paper.

REFERENCES

- [1] G. ALEFELD, AND G. MAYER, *Interval analysis: Theory and applications*, J. Comput. Appl. Math., 121 (2000), pp. 421–464.
- [2] V.M. ALEXEEV, *On the capture orbits for the three-body problem for negative energy constant*, Uspekhi Mat. Nauk., 24 (1969), pp. 185–186.
- [3] K.T. ALLIGOOD, T.D. SAUER, AND J.A. YORKE, *Chaos. An Introduction to Dynamical Systems*, Springer, Berlin, 1997.
- [4] B. BÁNHÉLYI, T. CSENDES, AND B.M. GARAY, *Optimization and the Miranda approach in detecting horseshoe-type chaos by computer*, Int. J. Bifurc. Chaos, 17 (2007), pp. 735–747.
- [5] B. BÁNHÉLYI, T. CSENDES, AND B.M. GARAY, *Σ_2 -chaos for iterates of the classical Hénon mapping*, 2008, (in preparation).
- [6] E. BOSETTO, AND E. SERRA, *A variational approach to chaotic dynamics in periodically forced nonlinear oscillators*, Ann. IHP Anal. Non Linéaire, 17 (2000), pp. 673–709.
- [7] A. CAPIETTO, W. DAMBROSIO, AND D. PAPINI, *Superlinear indefinite equations on the real line and chaotic dynamics*, J. Differ. Eq., 181 (2002), pp. 419–438.
- [8] L.O. CHUA, AND T. ROSKA, *Cellular neural networks and visual computing*, Cambridge University Press, Cambridge, 2002.
- [9] B.A. COOMES, H. KOCAK, AND K.J. PALMER, *Homoclinic shadowing*, J. Dynam. Differ. Eq., 17 (2005), pp. 175–215.
- [10] T. CSENDES, B.M. GARAY, AND B. BÁNHÉLYI, *A verified optimization technique to locate chaotic regions of a Hénon system*, J. of Global Optimiz., 35 (2006), pp. 145–160.
- [11] S. DAY, R. FRONGILLO, AND R. TREVINO, *Algorithms for rigorous entropy bounds and symbolic dynamics*, submitted.
- [12] M. DELLNITZ, G. FROYLAND, AND O. JUNGE, *The algorithms behind GAIO-set oriented numerical methods for dynamical systems*, in *Ergodic Theory, Analysis, and Efficient Simulation of Dynamical Systems*, (ed. by B. Fiedler), Springer, Berlin, 2001, pp. 145–174.
- [13] M. DELLNITZ, AND O. JUNGE, *Set oriented numerical methods for dynamical systems*, in *Handbook of Dynamical Systems, Vol. 2*, (ed. by B. Fiedler), North-Holland, Amsterdam, 2002, pp. 221–264.
- [14] V. FRANCESCHINI, AND L. RUSSO, *Stable and unstable manifolds of the Hénon mapping*, J. Statist. Phys., 25 (1981), pp. 757–769.
- [15] A. FROMMER, AND B. LANG, *Existence tests for solutions of nonlinear equations using Borsuk's theorem*, SIAM J. Numer. Anal., 43 (2005), pp. 1348–1361.
- [16] A. FROMMER, B. LANG, AND M. SCHNURR, *A comparison of the Moore and Miranda existence tests*, Computing, 72 (2004), pp. 349–354.
- [17] M. FURI, M. MARTELLI, M. O'NEIL, AND C. STAPLES, *Chaotic orbits of a pendulum with variable length*, Electron. J. Differ. Eq., No.36 (2004), pp. 14.
- [18] Z. GALIAS, *Positive topological entropy of Chua's circuit: a computer-assisted proof*, Int. J. Bifurc. Chaos, 7 (1997), pp. 331–349.
- [19] Z. GALIAS, *Obtaining rigorous bounds for topological entropy for discrete time dynamical systems*, in *Proc. Int. Symp. on Nonlinear Theory and its Applications* (Xi'an, China), 2002, pp. 619–622.
- [20] Z. GALIAS, AND P. ZGLICZYNSKI, *Abundance of homoclinic and heteroclinic orbits and rigorous bounds for the topological entropy for the Hénon map*, Nonlinearity, 14 (2001), pp. 909–932.

- [21] M. GIDEA, AND P. ZGLICZYNSKI, *Covering relations for multidimensional dynamical systems*, J. Differ. Eq., 202 (2004), pp. 32–58.
- [22] B. HASSARD, B. ZHANG, S.P. HASTINGS, AND W.C. TROY, *A computer proof that the Lorenz equations have “chaotic” solutions*, Appl. Math. Lett., 7 (1994), pp. 79–83.
- [23] S.P. HASTINGS, AND J.B. MCLEOD, *Chaotic motion of a pendulum with oscillatory forcing*, Amer. Math. Monthly, 100 (1993), pp. 563–572.
- [24] J.H. HUBBARD, *The forced damped pendulum: chaos, complication and control*, Amer. Math. Monthly, 106 (1999), pp. 741–758.
- [25] J.A. KENNEDY, S. KOCAK, AND J.A. YORKE, *A chaos lemma*, Amer. Math. Monthly, 108 (2001), pp. 411–423.
- [26] U. KIRCHGRABER, AND D. STOFFER, *On the definition of chaos*, Z. Angew. Math. Mech., 69 (1989), pp. 175–185.
- [27] O. KNÜPPEL, *PROFIL/BIAS – a fast interval library*, Computing 53 (1994), pp. 277–287.
- [28] M. LEVI, *Qualitative analysis of the periodically forced relaxation oscillations*, Mem. Amer. Math. Soc. 32 (1981) no. 244, pp. 147.
- [29] S. LUZZATTO, I. MELBOURNE, AND F. PACCAUT, *The Lorenz attractor is mixing*, J. Comm. Math. Phys., 260 (2005), pp. 393–401.
- [30] K. MISCHAIKOW, AND M. MROZEK, *Chaos in the Lorenz equations: a computer-assisted proof*, Bull. Amer. Math. Soc., 32 (1995), pp. 66–72.
- [31] M. MISIUREWICZ, AND B. SZEWC, *Existence of a homoclinic point for the Hénon mapping*, Comm. Math. Phys., 75 (1980), pp. 285–291.
- [32] N.S. NEDIALKOV, *VNODE – A validated solver for initial value problems for ordinary differential equations*, 2001. Available at www.cas.mcmaster.ca/~nedialk/Software/VNODE/VNODE.shtml
- [33] N.S. NEDIALKOV, K.R. JACKSON, AND G.F. CORLISS, *Validated solutions of initial value problems for ordinary differential equations*, Appl. Math. Comput., 105 (1999), pp. 21–68.
- [34] D. PAPINI, AND F. ZANOLIN, *Fixed points, periodic points, and coin-tossing sequences for mappings defined on two-dimensional cells*, Fixed Point Theory and Appl., 2 (2004), pp. 113–134.
- [35] D. PAPINI, AND F. ZANOLIN, *Some results on periodic points and chaotic dynamics arising from the study of the nonlinear Hill equation*, Rend. Sem. Mat. Univ. Pol. Torino, 2007, (in print).
- [36] L.C. PICCININI, G. STAMPACCIA, AND G. VIDOSSICH, *Ordinary Differential Equations in \mathbb{R}^n* , Springer, Berlin, 1984.
- [37] M. PIREDDU, AND F. ZANOLIN, *Fixed points for dissipative-repulsive systems and topological dynamics of mappings defined on N -dimensional cells*, Advanced Nonlinear Studies, 5 (2005), pp. 411–440.
- [38] A. POKROVSKII, O. RASSKAZOV, AND D. VISETTI, *Homoclinic trajectories and chaotic behaviour in a piecewise linear oscillator*, Discrete Cont. Dyn. Syst. Ser. B 8 (2007), pp. 943–970.
- [39] H. RATSCHKE, AND J. ROKNE, *New Computer Methods for Global Optimization*, Ellis Horwood, Chichester, 1988.
- [40] C. ROBINSON, *Dynamical Systems. Stability, Symbolic Dynamics, and Chaos*, RCR Press, Boca Raton, 1999.
- [41] J. RUBIN, AND D. TERMAN, *Geometric singular perturbation analysis of neuronal dynamics*, in *Handbook of Dynamical Systems Vol. 2*, ed. Fiedler, B., North-Holland, Amsterdam, 2002, pp. 93–146.
- [42] M. SCHNURR, *On the proofs of some statements concerning the theorems of Kantorovich, Moore and Miranda*, Reliable Comp., 11 (2005), pp. 77–85.
- [43] S. SMALE, *The Mathematics of Time*, Springer, Berlin, 1980.
- [44] D. STOFFER, AND K.J. PALMER, *Rigorous verification of chaotic behaviour of maps using validated shadowing*, Nonlinearity, 12 (1999), pp. 1683–1689.
- [45] S. TERRACINI, AND G. VERSINI, *Solutions of prescribed number of zeroes to a class of superlinear ODE’s systems*, NODEA Nonlin. Differ. Equat. Appl., 8 (2001), pp. 323–341.
- [46] W. TUCKER, *A rigorous ODE solver and Smale’s 14th problem*, Found. Comput. Math., 2 (2002), pp. 53–117.
- [47] X.S. YANG, AND Q. LI, *A computer-assisted proof of chaos in Josephson junctions*, Chaos Solitons Fractals, 27 (2006), pp. 25–30.
- [48] S. WIGGINS, *On the detection and dynamical consequences of orbits homoclinic to hyperbolic periodic orbits and normally hyperbolic invariant tori in a class of ordinary differential equations*, SIAM. J. Applied Math., 48 (1988), pp. 262–285.
- [49] S. WIGGINS, *Introduction to Applied Nonlinear Dynamical Systems and Chaos*, Springer, Berlin, 2003.

- [50] X.S. YANG, AND Q. LI, *A horseshoe in a cellular neural network of four-dimensional autonomous ordinary differential equations*, Int. J. Bifurc. Chaos, 17 (2007), pp. 3211–3218.
- [51] E. ZEIDLER, *Nonlinear Functional Analysis and its Applications. I. Fixed-point Theorems*, Springer, Berlin, 1986.
- [52] P. ZGLICZYNSKI, *Fixed point index for iterations of maps, topological horseshoe and chaos*, Topol. Methods Nonlin. Anal., 8 (1996), pp. 169–177.
- [53] P. ZGLICZYNSKI, *Computer assisted proof of chaos in the Rössler equations and in the Hénon map*, Nonlinearity, 10 (1997), pp. 243–252.
- [54] P. ZGLICZYNSKI, *Multidimensional perturbations of one-dimensional maps and stability of Sharkovski ordering*, Int. J. Bifurc. Chaos, 9 (1999), pp. 1867–1876.